



Contents lists available at SciVerse ScienceDirect

Organic Electronics

journal homepage: www.elsevier.com/locate/orgel

Electronic properties associated with conformational changes in azobenzene-derivative molecular junctions

Yonghun Kim^a, Gunuk Wang^a, Minhyeok Choe^a, Juhwan Kim^a, Sangchul Lee^b, Sungjun Park^a, Dong-Yu Kim^{a,b}, Byoung Hun Lee^{a,b}, Takhee Lee^{c,*}^aSchool of Materials Science and Engineering, Gwangju Institute of Science and Technology, Gwangju 500-712, Republic of Korea^bDepartment of Nanobio Materials and Electronics, Gwangju Institute of Science and Technology, Gwangju 500-712, Republic of Korea^cDepartment of Physics and Astronomy, Seoul National University, Seoul 151-747, Republic of Korea

ARTICLE INFO

Article history:

Received 28 April 2011

Received in revised form 11 August 2011

Accepted 25 August 2011

Available online 21 September 2011

Keywords:

Molecular electronic devices

Molecular configuration

Azobenzene

Photoisomerization

ABSTRACT

The electronic properties of azobenzene-derivative ([4-(phenylazo)phenoxy]hexane-1-thiol) molecular junctions were studied in terms of their molecular configurations with vertical device structure as solid-state device platform. This molecule has two distinct molecular configurations (trans- and cis-isomer) depending on the wavelength of irradiating light, which converts from more thermodynamically stable trans-isomer to cis-isomer under UV exposure (~365 nm) and reversible photoisomerization of cis-isomer to trans-isomer under visible light (400–500 nm). The two states showed that the conductance of cis-isomer (compact form) was higher than that of trans-isomer (extended form). From the temperature-variable electrical characterization, the main charge conduction mechanism for the two isomers was found to be tunneling. And, from the transition voltage spectroscopy analysis and ultraviolet photoelectron spectroscopy measurement, the origin of such result can be explained by reduction of molecular tunneling distance between two isomers.

© 2011 Elsevier B.V. All rights reserved.

1. Introduction

The understanding and control of charge transport through metal–molecule–metal junctions is a key factor for the realization and implementation of molecular electronic components, such as transistors, diodes, and switches in semiconductor-based electronic circuits [1–3]. Molecular switches are addressed by an electric field, external light, or chemical reactions between two states [4–6]. In particular, molecular switching phenomena operated by conductance changes on exposure to an external light source have been studied due to their advantages including easy addressability, fast response time, and good thermal stability [7]. Azobenzene derivatives are some of the most frequently investigated molecular candidates for photoin-

duced switching applications. They can be interconverted from trans-isomer to cis-isomer upon ultraviolet (UV) irradiation (~365 nm) and also interchanged from cis-isomer to trans-isomer upon exposure to visible light (400–500 nm), which is known as trans-cis photoisomerization [8,9]. The photoisomerization of azobenzene derivatives has been performed by various methods. For example, the conductance switching of thiolated azobenzene self-assembled monolayers (SAMs) on Au(111) was studied by conducting atomic force microscopy (CAFM) [10]. This phenomenon was caused by the conductance changes of the trans- and cis-isomers on exposure to different wavelengths of light; a higher conductance of the cis-isomer than that of the trans-isomer was reported and explained by the difference in tunneling distances. Moreover, the trans-cis photoisomerization of azobenzene-derivative molecular junctions on a Au(111) surface was demonstrated using scanning tunneling microscopy (STM) [11].

* Corresponding author. Tel.: +82 2 880 4269; fax: +82 2 884 3002.

E-mail address: tlee@snu.ac.kr (T. Lee).

However, in terms of more practical device applications, solid-state device structure is more preferable to CAFM or STM testbeds [12]. Furthermore, with CAFM or STM tools, it is not trivial to perform temperature-variable electrical characterizations to investigate charge conduction mechanisms, and it is generally difficult to determine the actual contact junction area. Therefore, a more comprehensive study based on a statistical analysis of the electrical properties induced by conformational changes in azobenzene-derivative molecules using a solid-state device structure is important for understanding the conduction mechanism and for more practical device applications.

In this study, we report the electrical properties of azobenzene-derivative ([4-(phenylazo)phenoxy]hexane-1-thiol) molecular junctions in which the azobenzene moiety is linked to an alkanethiol (with six carbon atoms). Specifically, we studied the photo-induced conductance changes between the trans- and cis-isomers of this molecule through statistical analysis. The absorption spectrum was determined by UV–Vis spectroscopy to confirm the conformational changes between trans- and cis-isomers by an external light trigger. In addition, temperature-variable electrical characterization and transition voltage spectroscopy analysis were performed to understand the charge transport mechanisms in both isomers.

2. Experimental

As schematically described in Fig. 1a, the molecular junctions were fabricated on a p-type Si (100) substrate covered by a thermally grown 6000 Å-thick SiO₂ layer. Conventional optical lithography was used to pattern the bottom electrodes prepared from Au (800 Å)/Ti (50 Å) using an electron-beam evaporator. Photoresist (PR) (AZ1512) was spin-coated on top of the bottom electrodes for electrical isolation. After isolation, square holes with side length of 30–100 μm were created through PR layer by optical lithography to expose the Au bottom electrodes. The devices with PR patterns were then annealed for at least 2 h at 180 °C to make the PR layer insoluble in ethanol during the formation of self-assembled monolayers (SAMs) on the Au bottom electrode. We used an azobenzene-derivative ([4-(phenylazo)phenoxy]hexane-1-thiol) consisting of two phenyl rings linked by an N=N double bond. These azobenzene-derivative molecules have two distinct isomers: trans- (extended form) and cis-isomer (compact form) depending on the wavelength of irradiating light (Fig. 1d). We prepared trans- and cis-isomer devices in the following way. First, SAMs (~1 mM) of trans-isomer were formed on the Au bottom electrode in a nitrogen-filled glove box with an oxygen level less than ~10 ppm for 1–2 days under visible light irradiation (400–500 nm). After the formation of trans-isomer azobenzene SAMs, several devices were illuminated by UV light (365 nm) in a darkroom for one hour, a period of time sufficient to guarantee a complete conformational change from the trans- to cis-isomer. Next, poly(3,4-ethylene-dioxythiophene) stabilized with poly(4-styrenesulphonic acid) (PEDOT:PSS) was spin-coated onto the tops of all devices to prevent electrical shorts between bottom Au electrode and a deposited Au top electrode [13,14]. The Au top electrode was deposited

through a shadow mask using the electron-beam evaporator, which acted as a self-aligned etching mask during the removal of exposed PEDOT:PSS. Finally, the remaining PEDOT:PSS outside the junctions was removed by reactive ion etching using O₂ gas.

The current–voltage (*I*–*V*) characterization of the fabricated molecular devices was carried out using a probe station and a semiconductor parameter analyzer (HP4155A) in ambient air at room temperature. And, the temperature variable *I*–*V* characterization was also performed in a cryostat system (ST-100 from Janis Co.) at the temperature ranging from 77 to 290 K. The absorption spectra of the azobenzene-derivative molecules in chloroform were characterized by using a UV–Vis spectroscopy measurement (PerkinElmer Lambda 750).

3. Results and discussion

3.1. photo-induced isomers

The photo-induced isomers of azobenzene derivatives are distinguished by the different physical and optical properties of the two configurations (trans- and cis-isomers), which can be observed through changes in their respective absorption spectra, dipole moments, refractive indices, and molecular conformations [15,16]. Before fabricating molecular devices, we measured the absorption spectra of the azobenzene derivative in chloroform to confirm the conformational changes upon external light irradiation. Fig. 2a shows the absorption spectra of our azobenzene derivatives in chloroform using UV–Vis spectroscopy. Generally, the absorption spectra of azobenzene derivatives are characterized by two distinct band peaks consisting of an intense band peak near 350 nm (UV region) and a weak band peak between 400 and 450 nm (visible region) [17]. The absorption transition near 350 nm is denoted as the $\pi\pi^*$ transition, which represents the rotation motion of the upper phenyl ring at the site of the N=N double bond for the trans-cis photoisomerization process. The absorption transition between 400 and 450 nm is denoted as the $n\pi^*$ transition, which represents the inversion motion of the upper phenyl ring at the same site [18]. The $n\pi^*$ transition is known to be prohibited for the trans-isomer, but it is allowed for the cis-isomer [19]. However, although the $n\pi^*$ transition of the trans-isomer is originally forbidden, a small amount of $n\pi^*$ transition peak is observed due to vibronic coupling between the $n\pi^*$ and $\pi\pi^*$ states [19].

In the trans-isomer, the two band peaks near 350 nm and between 400 and 450 nm were observed by UV–Vis spectroscopy (the blue curve in Fig. 2a). The $\pi\pi^*$ transition peak is relatively dominant compared with the $n\pi^*$ transition peak. After the trans-isomer was irradiated with UV light for 90 min in a darkroom, the intensity of the $n\pi^*$ transition peak increased because the $n\pi^*$ transition is allowed for the cis-isomer, and the $\pi\pi^*$ transition peak decreased (however, it was still intense compared with the $n\pi^*$ transition peak). From this photo-induced transition, we estimated the ratio of trans- to cis-photoisomerization from the spectra in solution. From the ratio of absorbance peak between trans- and cis-isomers at ~350 nm, the

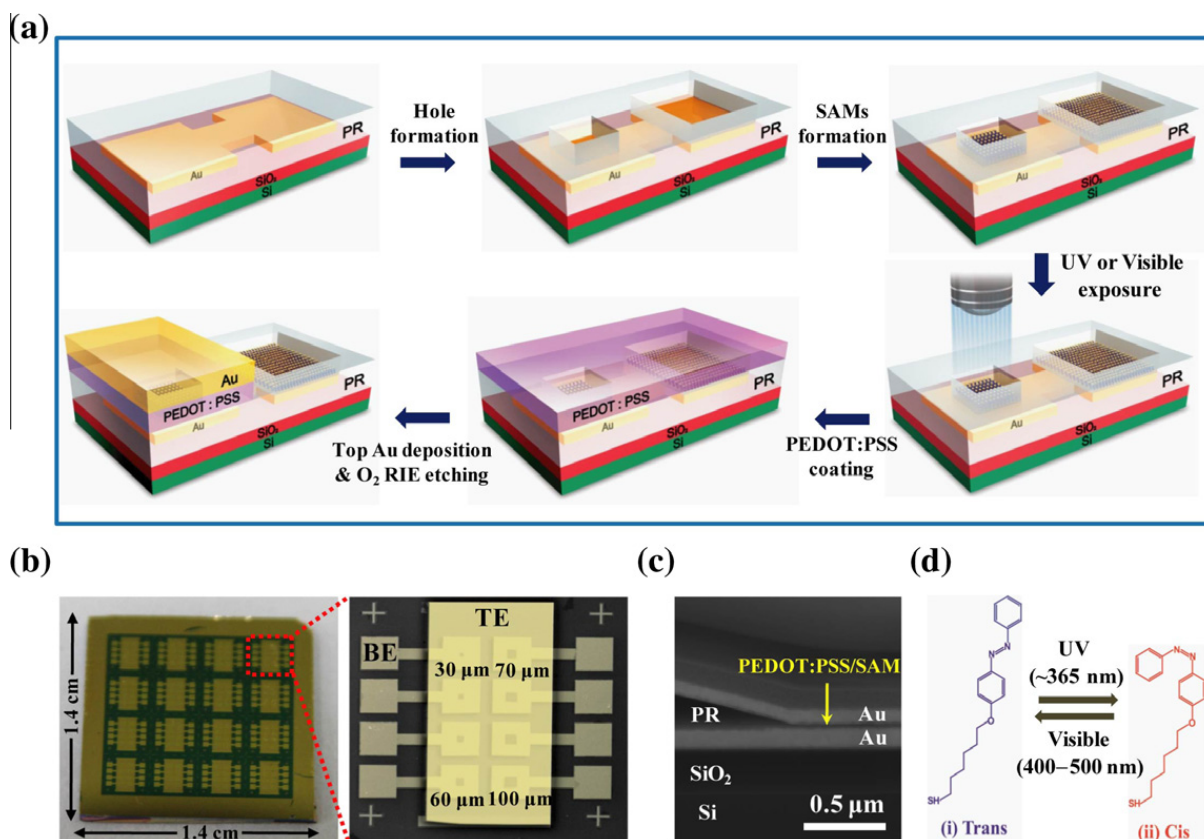


Fig. 1. (a) The process flow of device fabrication. (b) Photographic and SEM images of molecular junctions. A total of 128 junctions with square holes and side lengths of 30–100 μm are formed; BE and TE (yellow) denote the bottom and top electrodes, respectively. (c) Cross-sectional high-resolution SEM image of a molecular junction. (d) Molecular configurations of the trans- and cis-isomers. (For interpretation of the references to colour in this figure legend, the reader is referred to the web version of this article.)

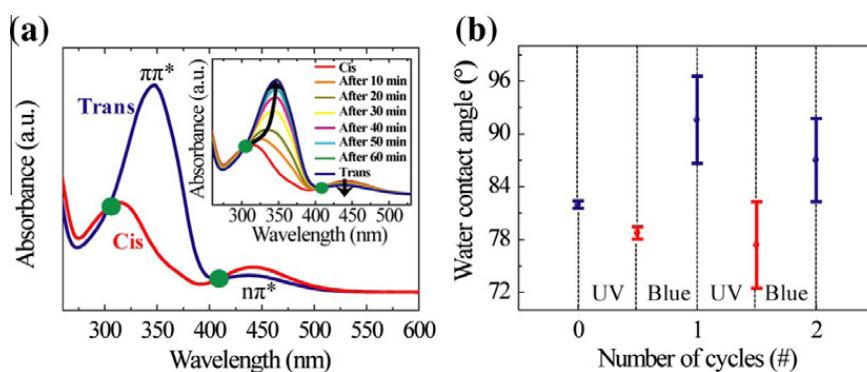


Fig. 2. (a) Absorption spectra of trans- (blue) and cis- (red) isomers in chloroform. Inset shows the evolution from cis- to trans-isomer upon visible light ($\sim 436\text{ nm}$) exposure. The two green circular symbols represent the isosbestic points. (b) The evolution of water contact angle of the trans-isomer (blue symbols) and cis-isomer (red symbols) on Au substrate after UV ($\sim 365\text{ nm}$) and blue light ($\sim 412\text{ nm}$) irradiation, respectively. (For interpretation of the references to colour in this figure legend, the reader is referred to the web version of this article.)

trans- to cis-isomerization was found to be $\sim 63\%$. This value suggests that all of the trans-isomers in solution are not completely changed to cis-isomers.

Furthermore, we investigated the conformational changes from the cis- to trans-isomer for the azobenzene derivative. Inset of Fig. 2a shows the evolution of the absorption spectrum of the cis-isomer (red curve) with visible light ($\sim 412\text{ nm}$) exposure at 10-min intervals. The $\pi\pi^*$ transition peak of the cis-isomer increased and the $n\pi^*$ transition peak decreased upon visible light irradiation.

After an hour of visible light irradiation, the cis-isomer was completely converted back into the trans-isomer. Note that the solvent of chloroform may evaporate during the UV–Vis measurement, but the effect of solvent evaporation would be negligible at least during the period of our measurement time, because the two isosbestic points did not change noticeably.

To elucidate the trans-cis photoisomerization behavior of azobenzene derivative on Au surface, it is necessary to confirm the conformational changes by external light. The

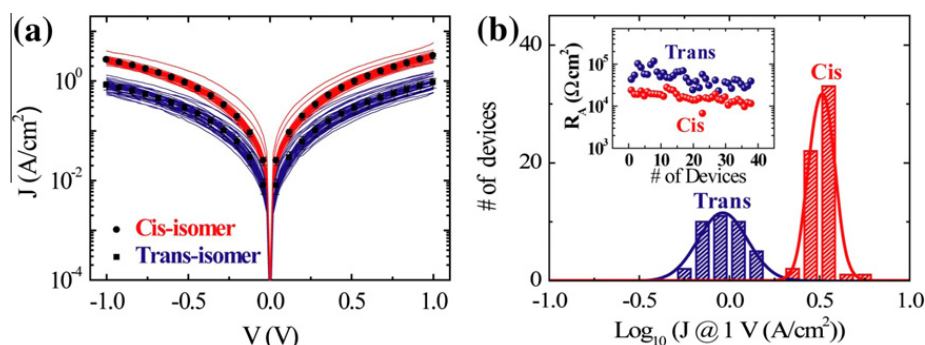


Fig. 3. (a) J - V curves on a logarithmic scale for trans-isomer (blue) and cis-isomer (red). The symbols and error bars represent the average and standard deviation of the current density for all the measured devices (~ 50 devices for each isomer case), respectively. (b) A histogram of J at 1 V for the trans- and cis-isomers. The solid lines are Gaussian fitting curves. The inset shows the distribution of the resistance-area products (R_A) for the trans- and cis-isomers. (For interpretation of the references to colour in this figure legend, the reader is referred to the web version of this article.)

evolution of the water contact angle on Au surface of azobenzene SAMs was monitored as a function of external irradiation wavelengths in Fig. 2b. Before UV light irradiation (~ 365 nm) on SAMs, the contact angle of pristine SAMs was about $81 \pm 0.4^\circ$. After UV light irradiation for 90 min in a dark room, the contact angle decreased to $78 \pm 0.6^\circ$, which is attributed to the trans- to cis-isomerization [21]. And, after subsequent visible light irradiation (~ 412 nm) for 90 min, the contact angle increased to $91 \pm 4^\circ$ due to cis- to trans-isomerization.

Also, we conducted the repeatable cycling measurements and confirmed the water contact angle values were reproducible for two cycles. This difference of water contact angle on trans- and cis-isomer on Au surface is mainly attributed to different top contact group and dipole moment [22]. The top contact group of trans-isomer is constituted by hydrophobic CH_3 group. In the cis-isomer, the azo ($\text{N}=\text{N}$ bond) or phenyl group is exposed by UV light irradiation. Therefore, the surface wettability for two isomers is different.

3.2. Electrical properties and charge transport mechanism

Using the metal-molecule-metal device structure shown in Fig. 1, we statistically studied the electrical properties of the two isomers. Fig. 3a shows the current density-voltage (J - V) characteristics of the trans- and cis-isomer-based molecular junctions. We plotted the J - V curves for ~ 50 molecular junctions of each isomer in Fig. 3a. The important point is that the current densities of the cis-isomer junctions were higher than those of the trans-isomer junctions. To statistically compare the electrical characteristics of the trans- and cis-isomers, histograms of the logarithmic current densities ($\log J$) at 1 V were plotted for both isomers, as shown in Fig. 3b. The histograms of the trans- and cis-isomer did not overlap (except for slight tails) and had distinct ranges of current density. The representative current densities were determined as the mean values of Gaussian fittings of the histograms and were found to be ~ 0.93 and 3.21 A/cm^2 for the trans-isomer and cis-isomer junctions, respectively. It is noted that the photoisomerization from trans- to cis-isomer might be suppressed in SAMs as compared with that in solution

because the azobenzene derivatives in self-assembled monolayers are highly densely packed and subsequently there is lack of free volume in the interior of the monolayers [20]. Therefore, it is considered that the ratio of photoisomerization in SAMs may become smaller than that in solution.

Because the junction areas were different in our case (with side lengths of 30–100 μm), we considered the product of the resistance (R) and area (A), i.e., $R_A (=R \times A)$, to be a junction-area-compensated quantity [23]. The obtained resistance-area products R_A of the trans- and cis-isomers were well distributed, as shown in the inset of Fig. 3b. The average R_A values were determined to be $(4.73 \pm 2.20) \times 10^4$ and $(1.40 \pm 0.40) \times 10^4 \Omega \text{ cm}^2$ for the trans- and cis-isomers, respectively.

To investigate the conduction mechanisms of the trans- and cis-isomers, a temperature-variable characterization was performed. Fig. 4a shows an Arrhenius plot [$\ln(J)$ versus $1/T$] with curves at different biases ranging from 0.6 to 1.0 V in increments of 0.1 V. The temperature was varied from 77 to 290 K in increments of 40 K. For the trans-isomer (top of Fig. 4a), there were no significant changes in the slopes of the Arrhenius curves as the temperature was varied. This temperature-independent behavior indicates that the main charge transport mechanism in the trans-isomer is a tunneling in the measured bias range [24]. For the cis-isomer (bottom of Fig. 4a), the Arrhenius plot also showed a negligible temperature dependence (except for a very slight dependence at high temperature), suggesting that the overall conduction mechanism in the cis-isomer is also tunneling. If tunneling is the main conduction mechanism, the junction current density varies exponentially with the distance of tunneling pathway. The current density (J) for the molecular junction is described as:

$$J = J_0 \exp(-\beta d) \quad (1)$$

where J_0 is a constant, d is the tunneling distance, and β is the tunneling decay factor that represents charge transport efficiency through the molecules [25].

The molecular tunneling distances of the trans- and cis-isomers between the two electrodes were estimated using the Cambridge Scientific Chem3D software at 22.73 and

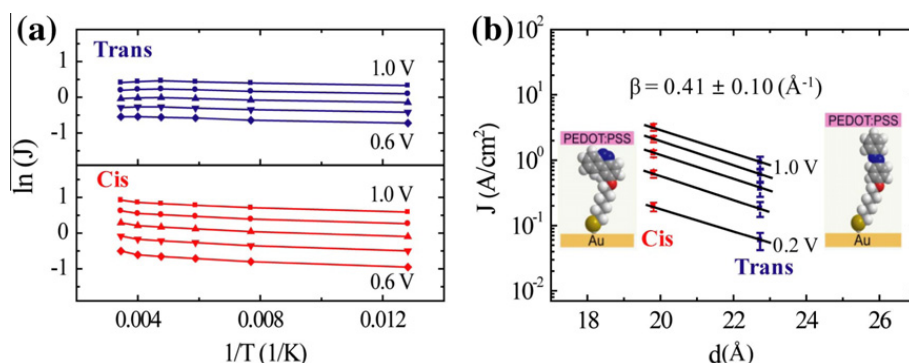


Fig. 4. (a) Arrhenius plot [$\ln(J)$ versus $1/T$] for the trans- and cis-isomers at different voltages ranging from 0.6 to 1.0 V (0.1 V step). (b) A semilog plot of J as a function of molecular tunneling distance (d) for the trans- and cis-isomers at different voltages. The slopes represent the tunneling decay factor β ($\sim 0.41 \text{ \AA}^{-1}$).

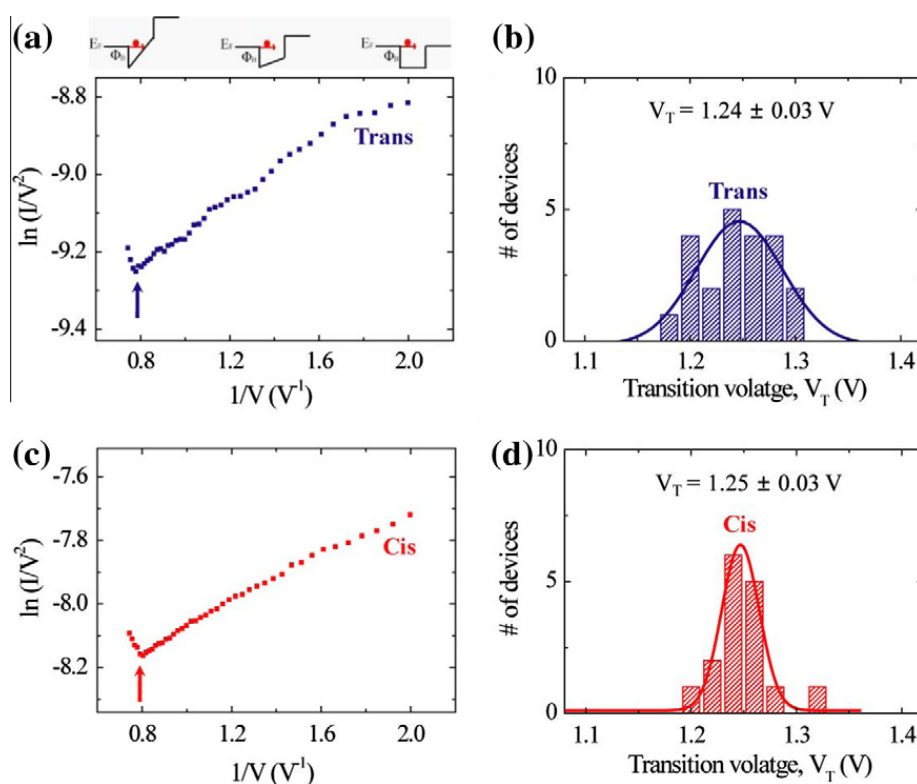


Fig. 5. (a and c) Representative plots of $\ln(I/V^2)$ versus $(1/V)$ for the trans- and cis-isomers. The arrows indicate the transition point from DT to FN tunneling for the trans- and cis-isomers. (b and d) The statistical histograms of transition voltage (V_T) for the trans- and cis-isomers.

19.81 \AA , respectively. Details of the determination of the molecular tunneling distances for the trans- and cis-isomers are provided in Fig. S2 in the Supplementary Data. Because the current density of the molecular tunneling junctions obeys (Eq. (1)), we plotted a semilog plot of the current density versus molecular tunneling distances for the trans- and cis-isomers, as shown in Fig. 4b. The estimated tunneling decay factor β was then obtained from the slopes [25] and found to be $0.41 \pm 0.10 \text{ \AA}^{-1}$ at different biases. The observed β value in our study is similar to previously reported values in the literature [26,27]. Note that there is a variation in tunneling distance between the two electrodes because of defects in molecular layer [28] and

imperfect interconversion of the molecules. Therefore, the experimental values of J are log-normally distributed as shown in Fig. 3b, and the estimated decay constant (β) represents the averaged degree of decay in our molecular junctions.

It is useful to analyze the tunneling transport with a conventional energy band model [29,30]. In the tunneling regime, when the applied bias is less than the barrier height ($V < \Phi_B/e$), charge transport exhibits direct tunneling (DT), and the barrier shape appears as a trapezoidal shape. On the other hand, when the applied bias is larger than the barrier height ($V > \Phi_B/e$), the charge transport is the field emission (or Fowler-Nordheim, FN) tunneling,

and the barrier shape appears as a triangular shape [29]. The important point is that the transition of the charge transport from DT to FN tunneling accompanies an inflection in a plot of $\ln(I/V^2)$ versus $(1/V)$ [30]. This inflection point is called the transition voltage (V_T), and this technique is termed transition voltage spectroscopy (TVS) [29,31]. The TVS method provides useful information about the location of the frontier molecular orbital (the highest occupied molecular orbital (HOMO) or lowest unoccupied molecular orbital (LUMO)) with respect to the Fermi level of the electrodes. Therefore, from the analysis of V_T by TVS characterization, one can estimate the energy offset between a metal electrode's Fermi energy and the frontier molecular orbital, which provides an estimated value of the barrier height (Φ_B); note V_T may not be identical to Φ_B . Plots of $\ln(I/V^2)$ versus $(1/V)$ for the trans-isomer (blue curve) and the cis-isomer (red curve) are shown in Fig. 5a and c, respectively (here, the applied bias was from 0 to 1.5 V). In the low-bias regime, this plot exhibits a logarithmic decay in the DT transport regime. Between the two charge transport regimes, an inflection point in the plot of $\ln(I/V^2)$ versus $(1/V)$ was observed (indicated by arrows). This inflection point is the transition voltage (V_T); it was determined to be ~ 1.25 V for both the trans- and cis-isomers (a small difference in V_T for the two isomers is within the error range). Fig. 5b and d shows statistical histograms for the V_T values of the trans- (22 devices) and cis-isomers (16 devices); Statistically, the V_T value was determined to be 1.24 ± 0.03 for the trans-isomer and 1.25 ± 0.03 V for the cis-isomer. This suggests that the energy offset, i.e., the barrier height (Φ_B), is also similar for both isomers regardless of the conformational change [32]. Note that the difference of conductance between the two isomers has also been reported in terms of the changes in their molecular electronic properties [33] (The details are described in the Supplementary Data).

To probe the positions of the HOMO levels of the SAMs on Au, we performed ultraviolet photoelectron spectroscopy (UPS) for each isomer. The UPS method has been used to estimate the work functions of metals and the HOMO levels of organic thin films [34,35]. We observed no significant difference between the HOMO levels of the trans- and cis-isomers on an Au substrate from the UPS measurements (for details, see Fig. S3 in the Supplementary Data). The UPS measurement result indicates that the electronic structure (HOMO level) of our molecule did not change on conversion from the trans- to the cis-isomer, meaning that the barrier height was also similar for the two isomers. Therefore, based on our study, we suggest that the main origin of the higher conductance of the cis-isomer is the difference in the molecular tunneling distance rather than the barrier height. This was confirmed by the fact that the V_T values of the trans- and cis-isomers are indeed similar: ~ 1.25 V (Fig. 5).

4. Conclusions

In conclusion, we performed a statistical study on the electrical characteristics of an azobenzene-derivative molecular junction in a solid-state device platform. This

molecule was reversibly converted from its trans- to cis-isomer by irradiation with UV light (~ 365 nm) and from its cis- to trans-isomer with visible light (400–500 nm). The conductance of cis-isomer (compact form) was higher than that of trans-isomer (extended form). From the temperature-variable electrical characterization, transition voltage spectroscopy analysis, and ultraviolet photoelectron spectroscopy measurement, the current density difference between the two isomers can be explained by the reduction in the molecular tunneling distance through the molecules sandwiched between the two electrodes.

Acknowledgements

This work was supported by the National Research Laboratory program; a Korean National Core Research Centre grant; the World Class University program of the Korean Ministry of Education, Science, and Technology; the Program for Integrated Molecular Systems at GIST. We thank Ja Min Koo and Yun Hee Jang for discussions throughout this study.

Appendix A. Supplementary data

Supplementary data associated with this article can be found, in the online version, at doi:10.1016/j.orgel.2011.08.017.

References

- [1] H. Song, Y. Kim, Y.H. Jang, H. Jeong, M.A. Reed, T. Lee, *Nature* 462 (2009) 1039.
- [2] K. Mohanta, A.J. Pal, *Org. Electron.* 10 (2009) 960.
- [3] D.W. Steuerman, H.-R. Tseng, A.J. Peters, A.H. Flood, J.O. Jeppesen, K.A. Nielsen, J.F. Stoddart, J.R. Heath, *Angew. Chem. Int. Ed.* 43 (2004) 6486.
- [4] M. Alemani, M.V. Peters, S. Hecht, K.-H. Rieder, F. Moresco, L. Grill, *J. Am. Chem. Soc.* 128 (2006) 14446.
- [5] A.S. Kumar, T. Ye, T. Takami, B.-C. Yu, A.K. Flatt, J.M. Tour, P.S. Weiss, *Nano Lett.* 8 (2008) 1644.
- [6] U. Pischel, *Angew. Chem. Int. Ed.* 46 (2007) 4026.
- [7] M. Irie, *Chem. Rev.* 100 (2000) 1685.
- [8] M.-M. Russev, S. Hecht, *Adv. Mater.* 22 (2010) 3348.
- [9] U. Jung, O. Filinova, S. Kuhn, D. Zargarani, C. Bornholdt, R. Herges, O. Magnussen, *Langmuir* 26 (2010) 13913.
- [10] J.M. Mativetsky, G. Pace, M. Elbing, M.A. Rampi, M. Mayor, P. Samorì, *J. Am. Chem. Soc.* 130 (2008) 9192.
- [11] G. Pace, V. Ferri, C. Grave, M. Elbing, C. von Hänisch, M. Zharnikov, M. Mayor, M.A. Rampi, P. Samorì, *Proc. Nat. Acad. Sci.* 104 (2007) 9937.
- [12] A.J. Kronemeijer, H.B. Akkerman, T. Kudernac, B.J. van Wees, B.L. Feringa, P.W.M. Blom, B. de Boer, *Adv. Mater.* 20 (2008) 1467.
- [13] H.B. Akkerman, P.W.M. Blom, D.M. de Leeuw, B. de Boer, *Nature* 441 (2006) 69.
- [14] P.A. Van Hal, E.C.P. Smits, T.C.T. Geuns, H.B. Akkerman, B.C. De Brito, S. Perissinotto, G. Lanzani, A.J. Kronemeijer, V. Geskin, J. Cornil, P.W.M. Blom, B. De Boer, D.M. De Leeuw, *Nat. Nanotechnol.* 3 (2008) 749.
- [15] C. Gahl, R. Schmidt, D. Brete, E.R. McNellis, W. Freyer, R. Carley, K. Reuter, M. Weinelt, *J. Am. Chem. Soc.* 132 (2010) 1831.
- [16] B.-Y. Choi, S.-J. Kahng, S. Kim, H. Kim, H.W. Kim, Y.J. Song, J. Ihm, Y. Kuk, *Phys. Rev. Lett.* 96 (2006) 156106.
- [17] K. Hoffmann, F. Marlow, J. Caro, *Adv. Mater.* 9 (1997) 567.
- [18] N. Tamai, H. Miyasaka, *Chem. Rev.* 100 (2000) 1875.
- [19] N. Biswas, S. Umaphathy, *Chem. Phys. Lett.* 236 (1995) 24.
- [20] J.-I. Anzai, S.-I. Sakasegawa, T. Takemura, T. Osa, *Mater. Sci. Eng. C2* (1994) 107.
- [21] N. Delorme, J.-F. Bardeau, A. Bulou, F. Poncin-Epaillard, *Langmuir* 21 (2005) 12278.
- [22] C.L. Feng, G. Qu, Y. Song, L. Jiang, D. Zhu, *Surf. Interface Anal.* 38 (2006) 1343.

- [23] G. Wang, T.-W. Kim, Y.H. Jang, T. Lee, J. Phys. Chem. C 112 (2008) 13010.
- [24] W. Wang, T. Lee, M.A. Reed, Phys. Rev. B 68 (2003) 035416.
- [25] I. Katsouras, V. Geskin, A.J. Kronemeijer, P.W.M. Blom, D.M. de Leeuw, Org. Electron. 12 (2011) 857.
- [26] V. Ferri, M. Elbing, G. Pace, M.D. Dickey, M. Zharnikov, P. Samorì, M. Mayor, M.A. Rampi, Angew. Chem. 120 (2008) 3455.
- [27] A. Salomon, D. Cahen, S. Lindsay, J. Tomfohr, V.B. Engelkes, C.D. Frisbie, Adv. Mater. 15 (2003) 1881.
- [28] C.A. Nijhuis, W.F. Reus, G.M. Whitesides, J. Am. Chem. Soc. 132 (2010) 18386.
- [29] J.M. Beebe, B. Kim, C.D. Frisbie, J.G. Kushmerick, ACS Nano 2 (2008) 827.
- [30] J.M. Beebe, B. Kim, J.W. Gadzuk, C.D. Frisbie, J.G. Kushmerick, Phys. Rev. Lett. 97 (2006) 026801.
- [31] E.H. Huisman, C.M. Guédon, B.J. van Wees, S.J. van der Molen, Nano Lett. 9 (2009) 3909.
- [32] S. Martin, W. Haiss, S.J. Higgins, R.J. Nichols, Nano Lett. 10 (2010) 2019.
- [33] K. Smaali, S. Lenfant, S. Karpe, M. Oçafrain, P. Blanchard, D. Deresmes, S. Godey, A. Rochefort, J. Roncali, D. Vuillaume, ACS Nano 4 (2010) 2411.
- [34] B.R. Chalamala, Y. Wei, R.H. Reuss, S. Aggarwal, B.E. Gnade, R. Ramesh, J.M. Bernhard, E.D. Sosa, D.E. Golden, Appl. Phys. Lett. 74 (1999) 1394.
- [35] B. Kim, J.M. Beebe, Y. Jun, X.-Y. Zhu, C.D. Frisbie, J. Am. Chem. Soc. 128 (2006) 4970.